

Nonponderomotive effects in multiphoton ionization of molecular hydrogen

Timo Wilbois* and Hanspeter Helm†

Department of Molecular and Optical Physics, University of Freiburg, Stefan-Meier-Str. 19, DE-79104 Freiburg, Germany

(Received 3 February 2011; published 12 May 2011)

Anomalous photoelectron angular distributions are observed at certain wavelengths in strong-field ionization of H_2 . We relate this feature to ac Stark shifts from bound-bound transitions in the Rydberg manifold of principal quantum number $n = 3$ and 4. A model of the multistate interaction supports this interpretation.

DOI: [10.1103/PhysRevA.83.053414](https://doi.org/10.1103/PhysRevA.83.053414)

PACS number(s): 33.80.Rv

I. INTRODUCTION

It is well known that atomic and molecular energy levels are shifted from their stationary state values in the presence of strong radiation fields, an effect commonly referred to as ac Stark shift [1,2]. On the other hand, a free electron in a radiation field is forced to a quiver motion. The cycle-averaged kinetic energy (ponderomotive energy) associated with this quiver motion is formidable at long wavelengths and high-field strength. Its value is given as $U_p = E^2/(4\omega^2)$, where E is the electric field amplitude and ω is the laser frequency, both in atomic units. U_p amounts to 0.934 eV at 10^{13} W/cm² at a wavelength of 1 μ m. In highly excited electronic states, the electron is for a substantial portion of time, far removed from the core, and suffers an equivalent quiver motion. Frequently, it is a good approximation to treat the ac Stark shift of highly excited states as ponderomotive, just as that of the ionization limit [3].

Purely ponderomotive shifting of Rydberg state energies is expected only in the case in which the wavelength is much longer than that of the first resonance transition from the ground state, but at the same time much shorter than any bound-bound transition among members of the Rydberg manifold. This was pointed out in early work on this topic by Avan *et al.* [4]. A prime example of nonponderomotive shifting was documented by Rottke *et al.* [5] in multiphoton ionization of atomic hydrogen using pulses of 500-fs duration. At wavelengths between 598 and 630 nm, near the Balmer- α line (656 nm), clear signals from ponderomotively shifted resonances of the type $4f$ and $5f$ are seen in their photoelectron spectra. However, contributions from lower-lying excited states appear at abnormal position and are broadened. The explanation is that the proximity of laser wavelength to the Balmer- α transition gives rise to anomalous ac Stark shifts of the $n = 2, 3$ states and this perturbation propagates to higher members of the Rydberg manifold (e.g., lifting the degeneracy of f and p states), as explained in their elaborate theoretical treatment [5].

Here, we report on similar observations in H_2 . The topic molecular hydrogen in strong laser fields has received continued attention in theory [6–12] and experiment [13–21]. A preponderance of short-pulse experiments on H_2 have been conducted at wavelengths near 800 nm, many concentrating on the question of Coulomb explosion, double ionization, and

molecular alignment. A few dealt explicitly with ac Stark shifting of intermediate resonance states [22–26].

The strongest visible and near-UV emission bands in molecular hydrogen are the $3d \leftrightarrow 2p$ and $4d \leftrightarrow 2p$ Rydberg-Rydberg transitions (see Fig. 1). The potential energy curves of singlet H_2 show the well-studied modification by long-range ion pair and doubly excited character, leading in some cases to double minima potentials. The lowest 11 Rydberg states of singlet H_2 are the $^1\Sigma_g^+$ states EF , GK , $H\bar{H}$, P , and O , the long-range ion pair state $B^1\Sigma_u^+$ and its higher analogs B' , B'' , and $B4$, and the $^1\Pi_u$ states C and D . We use the standard notation of Dressler and Wolniewicz [27], who calculated the potential energy curves shown in Fig. 1. Also shown in Fig. 1 is the vibrational wave function of ground state H_2 and its associated potential energy curve, both shifted up in energy by six photons of $\lambda = 470$ nm. We see that, at the energy of the six-photon dressed ground state, the states EF and GK are dissociative. Dominant contributions in $6 + 1$ photon ionization at 470 nm are thus expected from the resonant intermediate levels of the states $H\bar{H}$, P , and O , which we (in the following) refer to as the \mathcal{R} states. Similarly, at 330 nm, $4 + 1$ photon ionization involves the very same intermediate states.

Below, we show that signatures of the ac Stark shifting of these states and the associated state mixing of intermediate state resonances appear in the angle-resolved photoelectron distributions. A simplified model of strong-field ionization is used to explain our findings on the basis of the transition moments and potential energy curves calculated by Dressler and Wolniewicz [27].

II. EXPERIMENTAL RESULTS

We derive photoelectron momentum maps from Abel-inverted photoelectron images [28,29], recorded with the imaging spectrometer described in [30]. The maps give the electron momentum value as a function of emission angle, where the angle is measured relative to the linear laser polarization. Typical examples of photoelectron spectra that are dominated by intermediate resonances of the states discussed above are shown in Fig. 2. The spectra were recorded at a pulse length of ≈ 100 fs. The top of Fig. 2 refers to a wavelength of 470 nm. Nearly identical images are observed in the range from 470 to 485 nm, with the peak intensity being $\approx 3 \times 10^{13}$ W/cm². The prominent features are from $6 + 1$ photon ionization and at least four above-threshold ionization (ATI) channels. The bottom of Fig. 2 refers to a

*wilbois@cip.physik.uni-freiburg.de

†helm@uni-freiburg.de

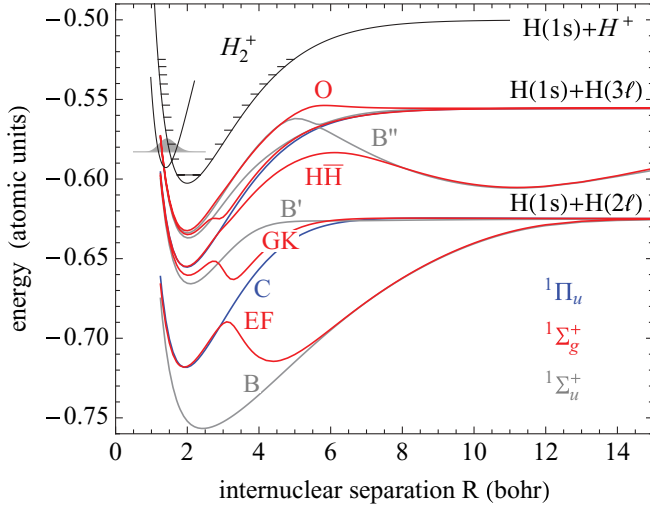


FIG. 1. (Color online) Potential energy curves of the lowest 11 Rydberg states of singlet molecular hydrogen, taken from Ref. [27] in relation to the ground-state potential of H_2^+ . The spatial extent of the H_2 ground-state vibrational wave function and associated potential energy curve are shown shifted by six-photon energies ($h\nu = 2.64$ eV).

wavelength of 332 nm, with the peak intensity being slightly lower, $\approx 2 \times 10^{13}$ W/cm². Here, the prominent ATI peaks are due to $4 + 1$ photon ionization and the respective ATI channels.

The above-threshold ionization features are easily recognized from the switching of nodal planes with increasing ATI number. As the minimum photon number used in the ionization process changes by one, so does the number of nodal

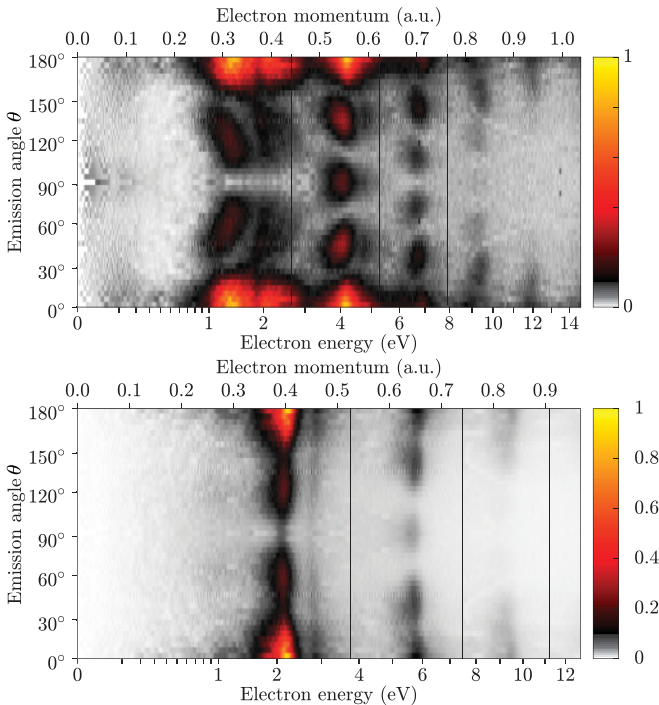


FIG. 2. (Color online) Angular distribution of electron momenta at 470 nm is shown in the top figure. Vertical black lines refer to the one-, two-, and three-photon energy above threshold $h\nu = 2.64$ eV. The result at 332 nm, $h\nu = 3.74$ eV, is shown in the bottom figure.

planes in the electron emission pattern, commensurate with the additional angular momentum imparted in the system. We expect that, at our laser pulse duration, the prominent features at energies below the one-photon energy (2.64 eV in Fig. 2) are due to one-photon ionization of ac Stark shifted excited states of the H_2 molecule. As the intensity in the pulse rises to a critical value (where n photons absorbed by the ground state reach an intermediate state resonance of ionization potential W_i), one-photon ionization of the intermediate state resonance produces electrons at $\epsilon_{\text{kin}} = h\nu - W_i$, with this drift energy being frozen out due to the short pulse [31,32].

We note that the strength of the ATI features is commensurate with the prediction of the free-free transition model of Delone and Krainov [33]. According to their model, the ratio of rates w of above-threshold ($K + 1$) photon ionization to threshold (K) photon ionization is

$$w^{(K+1)}/w^{(K)} = 0.14 E^2/\omega^{10/3}, \quad (1)$$

where E is the electric field strength and $\hbar\omega$ is the photon energy, both in atomic units. Equation (1) predicts ratios of 0.25 and 0.05 for the fields used at 470 and 332 nm, respectively, in agreement with the strength at which the first ATI features are observed in Fig. 2.

The anomalous curvature in angular distribution with electron energy initially caught our attention (see Fig. 2 top), as we are not aware of previous findings of this kind. The curvature points to a mechanism involving a range of intermediate resonance states with differing angular wave pattern of the outgoing electron. A more common appearance is the result obtained at 332 nm, where a fixed angular distribution appears for an isolated resonance channel.

Below, we attempt to illuminate this situation in a model simulation that utilizes the detailed knowledge available for singlet molecular hydrogen [27].

III. MODEL SIMULATION

To describe the contribution of intermediate state resonances to strong-field ionization, we diagonalize, at each value of internuclear separation R , the set of interacting dressed states described by the R -dependent Hamiltonian

$$\mathcal{H}(R) = \mathcal{H}_{\text{el}}^D(R) + \mathcal{H}_{\text{int}}(R). \quad (2)$$

The electronic Hamiltonian $\mathcal{H}_{\text{el}}^D(R)$ describes the potential energy curves of the five gerade states EF , GK , $H\bar{H}$, P , and O and the one-photon dressed ungerade states (C , D , and the four members of the B series). In the absence of interaction, these states are shown in Fig. 3 for the case $\lambda = 470$ nm. We see that, at this wavelength, the dressed B and C states are embedded in four higher $^1\Sigma_g^+$ states. Upon turning on the interaction, R -dependent ac Stark shifts will modify these potentials.

To describe the dipole interaction between the dressed states, we use the interaction Hamiltonian

$$\mathcal{H}_{\text{int}}(R) = \frac{\hbar}{2} g_{i,j}(R) + \text{H.c.}, \quad (3)$$

with the R -dependent Rabi-frequencies

$$g_{i,j}(R) = \frac{|d_{i,j}(R)| E_{\text{eff}}}{\hbar}. \quad (4)$$

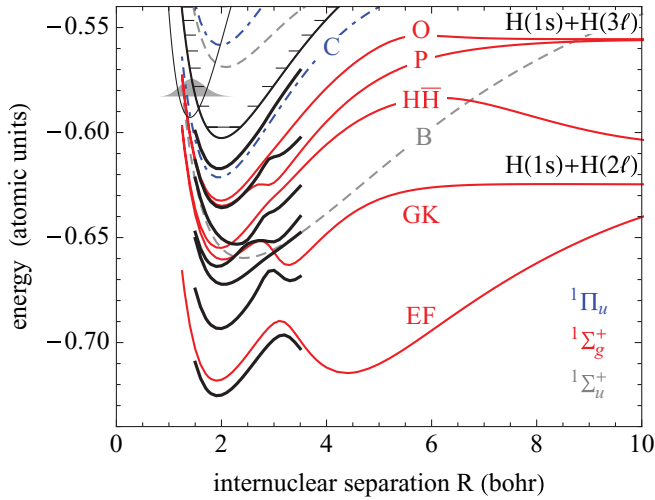


FIG. 3. (Color online) Dressed potential energy curves at 470 nm. Also shown are the six-photon dressed ground state of neutral hydrogen and the ground state of H_2^+ . The interacting states at $E_{\text{eff}} = 0.005$ a.u. are shown only in the region where the thicker lines are drawn.

The subscripts i and j label the interacting gerade and ungerade states and E_{eff} is the effective field strength of laser radiation. The R -dependent dipole moments $d_{i,j}(R)$ vary strongly with internuclear separation as may be seen in Fig. 2 of [34].

To estimate the effective field strength in our experiment E_{eff} , we consider the bandwidth of the laser radiation used $\Delta\nu = \pm 4$ THz at 470 nm (± 3 THz at 332 nm) in relation to the width of the Rydberg states. The natural lifetime of the states involved is typically of the order of 1 ns [35], however, one-photon ionization increases the width of the three higher-lying gerade states $H\bar{H}$, P , and O significantly. The bandwidth limiting factor is, however, most likely the two-photon ionization rate of the B $^1\Sigma_u^+$ state. This state acts as a main perturber at the wavelengths considered here, and it is difficult to assess a firm number for its width. We estimate E_{eff} to be about 10 times smaller than the bandwidth integrated field strength at 470 nm and about 8 times smaller at 332 nm. This is the sole free empirical factor in our model. We show in Fig. 3 the potentials in the presence of interaction at an effective field strength of 0.005 atomic units as black fat lines. For simplified viewing, we show the states in the presence of interaction only over a restricted range of internuclear separations.

A. Pattern of resonance energies

Excitation of the intermediate resonance states from the ground state of H_2 primarily probes their potential energy curves at short range, near $R = 1.5$ a.u., where the form of the relevant potentials is close to that of ground state H_2^+ . We therefore make the simplification that the Frank-Condon factors for transitions from ground state H_2 to H_2^+ also control the access of vibrational states in six-photon excitation. We further assume that the vibrational quantum number remains unchanged when these intermediate resonances are one-photon ionized, commensurate with previous observations

[36]. Thus, electrons formed in one-photon ionization of a vibronic state $\mathcal{R}(v)$,

$$\mathcal{R}(v) + h\nu \rightarrow H_2^+(v^+) + e + \epsilon_{\text{kin}}, \quad (5)$$

where $v = v^+$ produce photoelectrons at the kinetic energy $\epsilon_{\text{kin}} = W_{\mathcal{R}} + h\nu$, where $W_{\mathcal{R}}$ is the binding energy of the Rydberg at the equilibrium separation of ground state H_2^+ (≈ 2 a.u.).

We may estimate the rate of one-photon ionization of the resonant intermediate states using the generalized formula [37] for one-photon ionization of excited states with binding energy W_i :

$$\sigma_i = 8 \times 10^{-18} \sqrt{\frac{I_P}{W_i}} \left(\frac{W_i}{h\nu}\right)^3 [\text{cm}^2], \quad (6)$$

where I_P is the ground-state ionization potential of the species considered. We find $\sigma_i = 4.7 \times 10^{-18} \text{ cm}^2$ at 470 nm and $\sigma_i = 1.6 \times 10^{-18} \text{ cm}^2$ at 332 nm. Correspondingly, we have ionization rates of $(3 \text{ fs})^{-1}$ at 470 nm and $3 \times 10^{13} \text{ W/cm}^2$ and $(18 \text{ fs})^{-1}$ at 332 nm and $2 \times 10^{13} \text{ W/cm}^2$. It is, thus, safe to assume that ionization occurs practically instantly once a resonance is reached and a free electron is formed with a drift energy according to Eq. (5). As the pulse is too short to allow for any significant ponderomotive acceleration, this drift energy will be frozen out and observed at the detector [31,32]. We may, therefore, evaluate with the help of (5) the critical intensities at which specific vibrational levels of the \mathcal{R} states are shifted into resonance and predict the respective electron energy peaks. This occurs when the six- (four-) photon dressed ground state matches the ponderomotively shifted dressed state resonance. Denoting with I_P the ionization potential $H_2 X ^1\Sigma_g^+(v=0) \rightarrow H_2^+ X ^2\Sigma_g^+(v^+=0)$, and with V_{v^+} the energy of the vibrational level v^+ of the molecular ion ($V_0 = 0$), we have

$$N h\nu - I_P = W_{\mathcal{R}} + V_{v^+} + U_p(\mathcal{I}_c), \quad (7)$$

where $N = 6$ at wavelengths near 470 nm and $N = 4$ at wavelengths near 330 nm. From (7), we evaluate the critical intensities \mathcal{I}_c . These are marked in Fig. 4 by the points along the ac Stark shifted electronic state energies. Here, we use as energy scale $W_{\mathcal{R}} + h\nu$ as it is a direct measure of the electron energy expected in one-photon ionization of the intermediate state. We see that dominant ionization features are expected from the $^1\Sigma_g^+$ states O , P , and $H\bar{H}$. The dashed green curves are the EF and GK $^1\Sigma_g^+$ states, which are unbound at the six-photon (four-photon) energy and should thus only contribute to the dissociation channel. Two-photon transitions from the ungerade states (shown by the gray dashed lines in Fig. 4) could also contribute to the electron spectrum in this energy range, albeit at a much weaker level. We have therefore not included them in the simulation of the spectra. The respective angle-integrated electron energy spectra obtained in the experiment in the first channel above threshold are also shown in Fig. 4, at the right. The photoelectron spectra concentrate in the region where intermediate resonance states are predicted by our model.

In the experimental spectrum at 470 nm, contributions appear at very low energies $\epsilon < 0.2$ eV. We attribute this signal to six-photon nonresonant ionization. This channel

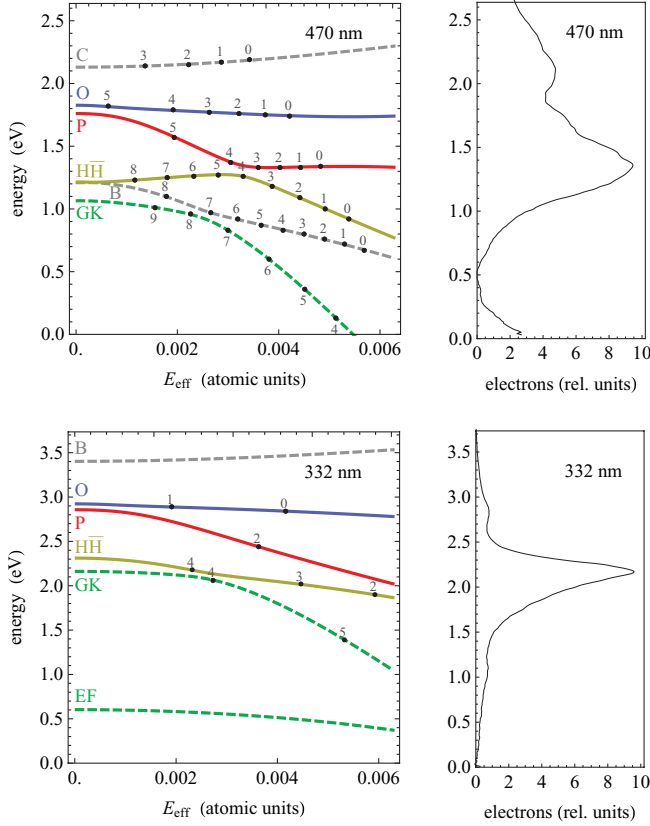


FIG. 4. (Color online) Resonances in the $1\Sigma_g^+$ states are marked by their vibrational quantum number. Lines give the respective state energies at $R = 2$ a.u., shifted up by one photon to also represent the kinetic energy spectrum. Dashed green lines correspond to dissociative states. The respective angle-integrated spectra are given at the right.

closes due to ponderomotive shifting at 1.9×10^{13} W/cm². The contribution at energies above 2 eV is attributed to Rydberg states with principal quantum number $n \geq 5$ rather than two-photon transitions from C -state intermediates. The $n \geq 5$ Rydberg states are not part of our 11-state model but are expected to deliver similar resonance contributions, albeit with lower signal as their excitation probability from ground state H_2 dilutes with n^{-3} [38].

A key test of the model will be to identify the strength at which each of the vibrational resonances in Fig. 4 actually contributes to the electron spectrum and its effect on the angular distribution. To carry this through in a precise fashion is a formidable task, which has not yet, to our knowledge, been undertaken. Therefore, we take the liberty to address this question in a very simplified, even simplistic model.

B. Strengths of resonances and angular pattern

The anomalous ac Stark shifting of states seen in Fig. 4 is accompanied by a strong variation of state amplitudes with laser intensity. This can be seen in Fig. 5 for a fixed internuclear separation $R = 2$ bohr. The state composition of each resonance channel controls the angular distribution of the outgoing photoelectron. This we consider next.

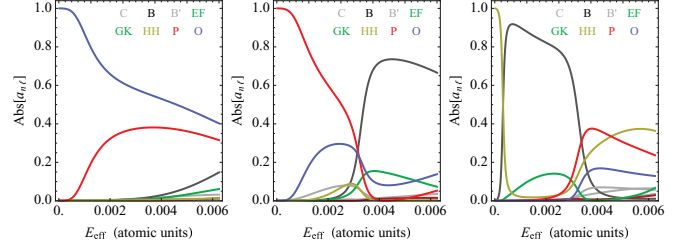


FIG. 5. (Color online) Squared amplitudes of the wave-function decomposition of the perturbed O , P , and HH states as a function of effective electric field strength at $R = 2$ bohr and at $\lambda = 470$ nm.

We describe the radial electronic wave function of the resonant intermediate states $R_{n\ell}$ by the one-center model wave functions given in [39] and estimate the transition dipole matrix element for one-photon ionization as

$$\langle n\ell|r|\epsilon\ell \pm 1 \rangle = \int_0^\infty R_{n\ell}(r) r^3 F_{k\ell \pm 1}(r) dr, \quad (8)$$

where $F_{k\ell}(r)$ is the Coulomb wave function for the free electron [40]. On this basis, we calculate the oscillator strength per unit atomic energy [41] for ionization of each intermediate Rydberg resonance, characterized by $n\ell$ and vibrational level $v = v^+$,

$$\frac{df}{d\epsilon} = \sum_{v^+, n, \ell} [f_{v^+} a_{n\ell} (\langle n\ell|r|\epsilon p \rangle + \langle n\ell|r|\epsilon f \rangle)]^2. \quad (9)$$

Here, f_{v^+} is the Frank-Condon factor for transitions between $v=0$ of ground state H_2 and a level v^+ of ground state H_2^+ , and $a_{n\ell}$ is the electronic amplitude of the Rydberg intermediate state. This amplitude is governed by the six-photon excitation process and hence, involves matrix element products [42] of the form $\langle 1s|r|np \rangle \langle np|r|n'\ell' \rangle \dots \langle n''\ell''|r|n\ell \rangle$, with the final values $\ell = 0, 2$ and $n = 3, 4, 5$. Considering the probability ratio for populating intermediate resonances with $\ell = 2$ (the state P) and $\ell = 0$ (the states HH and O), we see that this ratio is

$$A_{n''n} = \frac{a_{nd}}{a_{ns}} \propto \frac{\langle n''p|r|nd \rangle}{\langle n''p|r|ns \rangle}. \quad (10)$$

The pertinent values for this ratio in atomic hydrogen [43]¹ are near the value of 4, which we use in the following for all resonances. We also assume that the R -dependent and intensity-dependent resonance factors in the denominator for the six-photon transition matrix elements [42] are similar for all intermediate states such that they enter only as a scaling factor.

On this basis, we approximate the angular distribution of photoelectrons as a function of electron energy by

$$\frac{df}{d\epsilon d\theta} \approx \sum_{v^+, n, \ell} [f_{v^+} a_{n\ell} P_1^0(\theta) \langle n\ell|r|\epsilon p \rangle + P_3^0(\theta) \langle n\ell|r|\epsilon f \rangle]^2 \quad (11)$$

¹Hydrogenic values are $A_{2,3} = 5.0$, $A_{2,4} = 4.4$, $A_{2,5} = 4.3$, $A_{3,4} = 3.0$, $A_{3,5} = 3.1$, $A_{3,6} = 3.0$, $A_{4,5} = 3.3$, $A_{4,6} = 2.6$, taken from Ref. [43].

with $P_\ell^m(\theta)$ being the Legendre polynomials and θ the angle of the outgoing electron measured relative to the laser polarization axis. Neglecting rotational and spin angular momenta, we take $m = 0$, as linear laser polarization is used in our experiment.

C. Comparison with experiment

By folding the results of (10) with a spectral resolution of 10 meV, we obtain the high-resolution spectra shown in Fig. 6 in the top row at the left (470 nm, peak intensity 3×10^{12} W/cm²) and at the right (332 nm, peak intensity 2×10^{12} W/cm²). At this resolution, we recognize the individual resonance contributions, which are active at the two wavelengths.

The respective experimental spectra are given in the bottom row. An experimental energy resolution of about 50 meV is expected. Increasing the resolution to 100 meV, the spectra shown in the center row of Fig. 6 are obtained from our model simulation. This broadening delivers the best comparison to the experimental spectra. The extra broadening required to obtain agreement is a consequence of our assumption that

resonance ionization sets on sharply whenever an ac Stark shifted state is tuned into six-photon (four-photon) resonance. Obviously, this is a dynamic process with a width governed by intensity and laser bandwidth and it will therefore stretch the ionization feature over the scale of the photoelectron energies. The fundamental features of the simulation closely reproduce those observed in the experiment in the region between 0.2 and 2 eV at 470 nm and over the entire range at 332 nm. We note that, at 470 nm, comparison should only be made of the features below 2 eV, as contributions from higher Rydberg resonance states set in at 2.1 eV ($n \geq 5$), which are not part of the model. The same holds for the low electron energies $\epsilon < 0.2$ eV, where a nonresonant ionization channel is active at 470 nm as discussed above.

At 332 nm, where the peak intensity corresponds to $E_{\text{eff}} = 0.003$ atomic units, only two resonances participate prominently; these are the $v = 4$ level of $H\bar{H}$ and the $v = 1$ level of the O state. For both states, the effect of nonponderomotive shifting is minor at the limit of resolution of the experiment. On the other hand, at 470 nm, in the same range of effective field strengths, numerous resonance levels participate as seen from Fig. 4. These resonance positions are clearly different from those expected on the basis of purely ponderomotive shifting.

The curvature in the angular features at 470 nm, our original impetus to pursue this task, is not fully borne out by our current model. It is quite likely that contributions from higher angular momenta, which appear in the sequence of stimulated emission and stimulated absorption at these intensities, play a substantial role here.

IV. CONCLUSION

We show that the solid base of knowledge accumulated for molecular hydrogen can be utilized to predict fundamental features of the strong-field ionization response of this molecule. The deformation of intermediate resonance states in near-resonant excitation by the ionization laser field can be treated as adiabatic perturbation of the respective potential energy curves. In the cases considered here, intermediate states with $^1\Sigma_g^+$ character bear the dominant ionization pathways. Their treatment can be restricted to a single internuclear distance as they have potential curves that mimic that of the molecular ion. Application to intermediate states such as the $B^1\Sigma_u^+$ state will require a more explicit account of the vibrational amplitudes, but could otherwise follow similar considerations. A more complete catalog of the dynamic response of molecular hydrogen to strong laser fields, covering the range from 300 to 800 nm, is currently being accumulated in this laboratory. The concepts presented here form one of the cornerstones for interpretation of this catalog. The sample results given show that photoelectron imaging of short-pulse laser ionization can provide a direct view of the light-perturbed excited state structure of molecules.

ACKNOWLEDGMENTS

This work was supported by the Deutsche Forschungsgemeinschaft (Grant No. HE-2525/5). The authors wish to thank Professors H.-P. Breuer, J. S. Briggs, and A. Saenz for enlightening discussions.

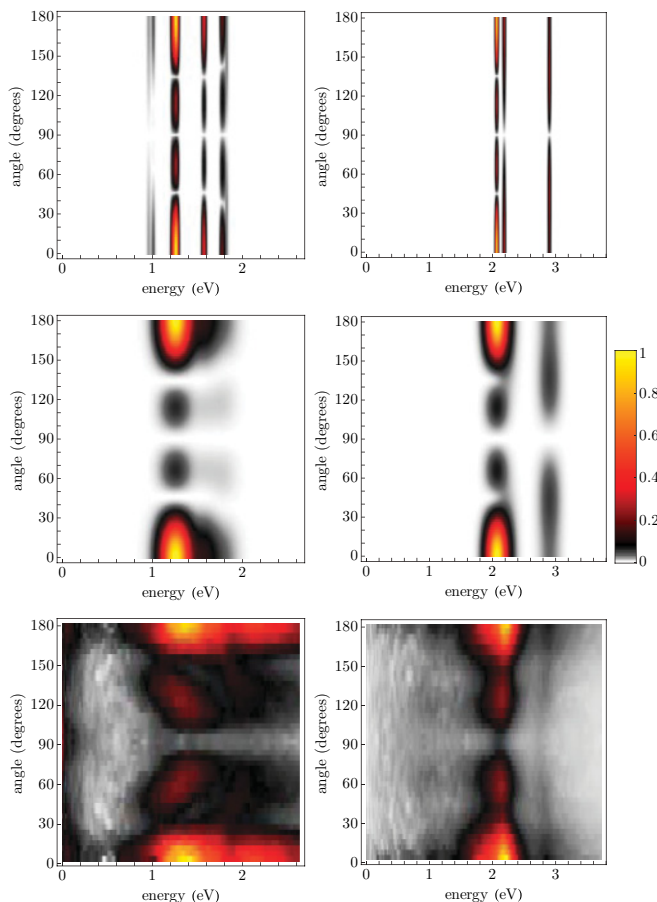


FIG. 6. (Color online) Results for 470 nm are given in the left column, and for 332 nm in the right column. The model simulation is given in the top row, at a resolution of 10 meV. The experimental results are shown in the bottom row. The center row gives the simulation result, artificially broadening the resonances in a Gaussian shape with $\sigma = 100$ meV. Only the region up to the energy of the first photon above threshold is shown, 2.64 and 3.73 eV, respectively. The high resolution image is shown with an image contrast of 0.5.

- [1] N. B. Delone and V. P. Krainov, *Usp. Fiz. Nauk.* **42**, 669 (1999) [*Phys. Usp.* **42**, 669 (1999)].
- [2] B. Girard, G. O. Sitz, R. N. Zare, N. Billy, and J. Vigue, *J. Chem. Phys.* **97**, 26 (1992).
- [3] R. R. Freeman, P. H. Bucksbaum, H. Milchberg, S. Darack, D. Schumacher, and M. E. Geusic, *Phys. Rev. Lett.* **59**, 1092 (1987).
- [4] P. Avan, C. Cohen-Tannoudji, J. Dupont-Roc, and C. Fabre, *J. Phys. (France)* **37**, 993 (1976).
- [5] H. Rottke, B. Wolff-Rottke, D. Feldmann, K. H. Welge, M. Dörr, R. M. Potvliege, and R. Shakeshaft, *Phys. Rev. A* **49**, 4837 (1994).
- [6] S. Chelkowski, T. Zuo, O. Atabek, and A. D. Bandrauk, *Phys. Rev. A* **52**, 2977 (1995).
- [7] A. Apalategui and A. Saenz, *J. Phys. B: At., Mol. Opt. Phys.* **35**, 1909 (2002).
- [8] Y. V. Vanne and A. Saenz, *Phys. Rev. A* **80**, 053422 (2009).
- [9] M. Awasthi and A. Saenz, *Phys. Rev. A* **81**, 063406 (2010).
- [10] K. Harumiya, I. Kawata, H. Kono, and Y. Fujimura, *J. Chem. Phys.* **113**, 8953 (2000).
- [11] K. Harumiya, H. Kono, Y. Fujimura, I. Kawata, and A. D. Bandrauk, *Phys. Rev. A* **66**, 043403 (2002).
- [12] L. A. A. Nikolopoulos, T. K. Kjeldsen, and L. B. Madsen, *Phys. Rev. A* **76**, 033402 (2007).
- [13] C. Cornaggia, D. Normand, J. Morellec, G. Mainfray, and C. Manus, *Phys. Rev. A* **34**, 207 (1986).
- [14] S. W. Allendorf and A. Szöke, *Phys. Rev. A* **44**, 518 (1991).
- [15] B. L. G. Bakker, D. H. Parker, and W. J. van der Zande, *Phys. Rev. Lett.* **86**, 3272 (2001).
- [16] A. S. Alnaser, T. Osipov, E. P. Benis, A. Wech, B. Shan, C. L. Cocke, X. M. Tong, and C. D. Lin, *Phys. Rev. Lett.* **91**, 163002 (2003).
- [17] J. H. Posthumus, *Rep. Prog. Phys.* **67**, 623 (2004).
- [18] X. Urbain, B. Fabre, E. M. Staicu-Casagrande, N. de Ruette, V. M. Andrianarijaona, J. Jureta, J. H. Posthumus, A. Saenz, E. Baldit, and C. Cornaggia, *Phys. Rev. Lett.* **92**, 163004 (2004).
- [19] W. Vanroose, F. Martin, T. N. Rescigno, and C. W. McCurdy, *Science* **310**, 1787 (2005).
- [20] C. Beylerian, S. Saugout, and C. Cornaggia, *J. Phys. B: At., Mol. Opt. Phys.* **39**, L105 (2006).
- [21] Th. Ergler, B. Feuerstein, A. Rudenko, K. Zrost, C. D. Schröter, R. Moshhammer, and J. Ullrich, *Phys. Rev. Lett.* **97**, 103004 (2006).
- [22] H. Pummer, H. Egger, T. S. Luk, T. Srinivasan, and C. K. Rhodes, *Phys. Rev. A* **28**, 795 (1983).
- [23] N. Bjerre, R. Kachru, and H. Helm, *Phys. Rev. A* **31**, 1206 (1985).
- [24] D. W. Chandler and L. R. Thorne, *J. Chem. Phys.* **85**, 1733 (1986).
- [25] H. Rottke, J. Ludwig, and W. Sandner, *Phys. Rev. A* **54**, 2224 (1996).
- [26] J. H. Posthumus, B. Fabre, C. Cornaggia, N. de Ruette, and X. Urbain, *Phys. Rev. Lett.* **101**, 233004 (2008).
- [27] K. Dressler and L. Wolniewicz, *Ber. Bunsenges. Phys. Chem.* **99**, 246 (1995).
- [28] H. Helm, N. Bjerre, M. J. Dyer, D. L. Huestis, and M. Saeed, *Phys. Rev. Lett.* **70**, 3221 (1993).
- [29] C. Bordas, F. Pauling, H. Helm, and D. L. Huestis, *Rev. Sci. Instrum.* **67**, 2257 (1996).
- [30] R. Wiehle, B. Witzel, H. Helm, and E. Cormier, *Phys. Rev.* **67**, 063405 (2003).
- [31] P. Agostini, J. Kupersztych, L. A. Lompre, G. Petite, and F. Yergeau, *Phys. Rev. A* **36**, 4111 (1987).
- [32] R. R. Freeman, P. H. Bucksbaum, and T. J. McIlrath, *IEEE J. Quantum Electron.* **24**, 1461 (1988).
- [33] N. B. Delone and V. P. Krainov, *Multiphoton Processes in Atoms* (Springer, Berlin, 2000), p. 152.
- [34] K. Dressler and L. Wolniewicz, *J. Mol. Spectrosc.* **96**, 195 (1982).
- [35] K. P. Huber and G. Herzberg, *Molecular Spectra and Molecular Structure* (Van Nostrand Reinhold, New York, 1979), Vol. IV.
- [36] H. Helm, M. J. Dyer, and H. Bissantz, *Phys. Rev. Lett.* **67**, 1234 (1991).
- [37] D. L. Huestis (private communication).
- [38] T. F. Gallagher, *Rydberg Atoms*, Cambridge Monographs on Atomic Molecular and Chemical Physics (Cambridge University, Cambridge, UK, 1994).
- [39] A. Lühr, Y. V. Vanne, and A. Saenz, *Phys. Rev. A* **78**, 042510 (2008).
- [40] H. Friedrich, *Theoretical Atomic Physics* (Springer, Heidelberg, 1996), p. 28.
- [41] S. T. Manson, C. J. Lee, R. H. Pratt, I. B. Goldberg, B. R. Tambe, and A. Ron, *Phys. Rev. A* **28**, 2885 (1983).
- [42] Y. Gontier and M. Trahin, in *Multiphoton Ionization of Atoms*, edited by S. L. Chin and P. Lambropoulos (Academic, Toronto, 1984).
- [43] H. A. Bethe and E. E. Salpeter, *Quantum Mechanics of One- and Two-Electron Atoms* (Plenum, New York, 1977).